

**The role of second metal  
on the catalytic in-situ generation of H<sub>2</sub>O<sub>2</sub>  
by Fe/Ni bimetallic nanoparticles:  
degradation studies of Metronidazole antibiotic**

Burçin YILDIZ<sup>1,\*</sup>, Ecehan ŞENER<sup>2</sup>, Özge HANAY<sup>2</sup>

<sup>1</sup>Department of Environmental Engineering, Faculty of Engineering, Van Yüzüncü Yıl University, 65080, Van, Turkey

<sup>2</sup>Department of Environmental Engineering, Faculty of Engineering, Firat University, 23119, Elazığ, Turkey

\*Corresponding author: Burçin Yıldız, e-mail: [burcinyildiz@yyu.edu.tr](mailto:burcinyildiz@yyu.edu.tr), ORCID: <https://orcid.org/0000-0001-9750-7278> Phone: +90 432 4445065-28235; Fax: +90 432 2251730

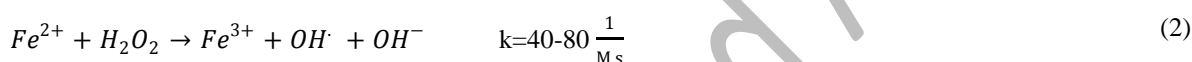
**ABSTRACT:** Fe-based bimetallic particles have been shown potential for Fenton process but the investigation of a second metal role on bimetallic particles remains challenging. In this study, nano sized Fe/Ni (nFe/Ni) particles were synthesized at different Ni loading rates (1, 3.5, 10 wt%) and used as catalyst for in-situ generation of H<sub>2</sub>O<sub>2</sub> by activating dissolved oxygen. Fenton process efficiency was defined via the degradation of a model organic pollutant as metronidazole (MNZ) antibiotic under different operational parameters. The experimental results indicate that the addition of Ni to nZVI particles with high loading significantly increased the production of H<sub>2</sub>O<sub>2</sub>, while low Ni loading rate resulted in high MNZ removal efficiency. The maximum removal efficiency of MNZ was about 99% obtained for 0.1 g/L nFe/Ni synthesized at 1% Ni loading rate at pH:3 within 1 hr. At pH:7, the MNZ removal was entirely due to adsorption, which was dependent on the catalyst dosage. In addition, the potential degradation products of MNZ were suggested based on the intermediates detected by LC-MS/MS. The conversion of MNZ to low and different molar mass intermediates confirmed the different degrees of MNZ degradation.

**KEYWORDS:** Heterogeneous Fenton, In-situ H<sub>2</sub>O<sub>2</sub>, Metronidazole, Nano Fe/Ni, Ni loading

## INTRODUCTION

The Fenton process, which is one of the advanced oxidation processes (AOPs), is very effective for oxidizing and mineralizing many refractory organic compounds due the formation of non-selective and highly reactive hydroxyl radicals ( $\cdot\text{OH}$ ). In the Fenton process, using the iron-based heterogeneous materials results in less sludge and the catalyst can be easily separated from the aqueous solution and reuse of the catalyst is usually possible [1]. Nano zero-valent iron (nZVI) particles are widely accepted due to their low toxicity, high specific surface area, and efficient vapor permeation [2]. Studies have shown that nZVI is an effective material for removing a variety of environmental contaminants, including organic solvents, dyes, metals, and mineral compounds [3].

However, the addition of nZVI to water containing dissolved oxygen (DO) results in the production of  $\text{H}_2\text{O}_2$  through a two-electron transfer from the particle surface to oxygen. (R.1) [1]. A solution of  $\text{Fe}^{2+}/\text{Fe}^{3+}$  and hydrogen peroxide ( $\text{H}_2\text{O}_2$ ), known as a Fenton reagent, promotes the formation of highly reactive  $\cdot\text{OH}$  (R.2) [4].



On the other hand, the in-situ generation of  $\text{H}_2\text{O}_2$  also offers an attractive alternative to external addition of  $\text{H}_2\text{O}_2$ , overcoming the considerable concerns such as high cost, handling, storing and transporting of concentrated  $\text{H}_2\text{O}_2$  [5]. Recent studies have suggested the available methods for in-situ continuous production of  $\text{H}_2\text{O}_2/\cdot\text{OH}$ , including photo-fenton, electro-Fenton and ZVI/ $\text{O}_2$  system [6-8]. Although high mineralization of organic compounds has been provided via  $\cdot\text{OH}$  generated by electro-Fenton and photo-Fenton, high cost of these processes hinder their large-scale applications. The in-situ generation of  $\text{H}_2\text{O}_2$  under oxic and acidic conditions by using nano zero valent iron (nZVI) have been demonstrated although the concentration of  $\text{H}_2\text{O}_2/\cdot\text{OH}$  produced in situ is still low to be utilized for the degradation of organic pollutants [9]. To enhance the  $\text{H}_2\text{O}_2$  generation in ZVI/oxygen systems, the particle surface structure can be modified by different approaches. For this purpose, bimetallic zero valent iron technology, in which Fe acts as the reducing agent along with the transition metals such as Cu, Ni, Ag and Pd incorporated to ZVI have been used [10-12]. The transition metal called as second metal plays different roles in bimetallic system due to facilitating the production of activated atomic hydrogen ( $\text{H}^*$ ) adsorbed on the bimetallic catalysts and enhancing the oxidation of ZVI through the formation of galvanic cells without an external power supply [13, 14]. The presence of atomic hydrogens enhances the reductive degradation of organic pollutants. The transition metal also improves the reactivity of ZVI by preventing the formation of iron hydroxide or hydroxide on the ZVI surface and the aggregation via Van der Waals and strong magnetic attraction forces of iron particles [15]. These competitive effects on the reactivity of ZVI changed with solution pH and particle surface structure [16].

To date many studies have focused on either the reductive degradation, precipitation and adsorption or oxidative degradation of many organic compounds (acetamiprid, ibuprofen, dyes, nitrobenzene, dichlorophenol, DDT) by using different bimetallic particles [11, 12, 17-20]. Although these studies could aid in understanding

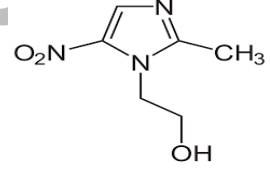
the function of bimetallic particles in removing the studied contaminants by evaluating the reaction conditions, (solution pH, catalyst dosage, concentration of contaminants and reaction time) a few studies about the effect of second metal loading rate on the iron elution and dissolved oxygen consumption which significantly influence the performance of oxygen-driven heterogeneous Fenton/ Fenton-like processes are available in the literature. For example, Wang et al. [21] found the increase of  $\bullet\text{OH}$  radical generation using Fe/Cu bimetallic nanoparticles with external addition of  $\text{H}_2\text{O}_2$  when Cu deposition was formed on iron. Yamaguchi et al. [14] evaluated in-situ generation of  $\text{H}_2\text{O}_2$  and  $\bullet\text{OH}$  radical depending on Cu loading rate by using Fe/Cu bimetallic nanoparticles in detail. They found that the loading of Cu on the ZVI surface hindered  $\bullet\text{OH}$  radical generation while the removal of Orange II enhanced via the enhancement of adsorption capability of Fe/Cu bimetallic. Therefore, it is still not clear the extent of second metal loading on the ZVI surface and there is a need for further study by using different metals. For this purpose, we choose Ni with a positive redox potential ( $E_0 = -0.25$  V) deposited on nano Fe (0) with a negative redox potential ( $E_0 = -0.44$  V) to improve the reactivity of the catalyst. Nickel is also low cost and shows good corrosion stability [17]. Hence, this work aimed to examine the effect of transition metal loading rate onto nZVI surface on in-situ generation of  $\text{H}_2\text{O}_2$  and  $\bullet\text{OH}$  radical by considering the oxygen consumption, iron elution and change in surface structure before and after the reaction and to determine the removal mechanism of Metronidazole (MNZ) antibiotic as a model organic pollutant. The initial parameters such as the value of solution pH and bimetallic dosage in the Fenton process were also investigated for MNZ degradation and removal of total organic carbon (TOC). Furthermore, the evolutions of the intermediates under the various nickel loading rates were monitored.

## EXPERIMENTAL SECTION

### Chemicals

The physicochemical properties of Metronidazole ( $\text{C}_6\text{H}_9\text{N}_3\text{O}_3$ ), was given in Table 1. It was purchased from Maybridge in 99% purity while reagent grades of  $(\text{NH}_4)_2\text{H}_2\text{PO}_4$  (98% purity),  $\text{NiCl}_2 \cdot 6\text{H}_2\text{O}$  (99.9% purity),  $\text{HClO}_4$  (70% purity),  $\text{NaOH}$  (98% purity) and  $\text{H}_2\text{SO}_4$  (95-98% purity) were purchased from Merck.

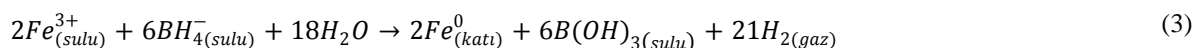
Table 1. The physicochemical properties of MNZ [22]

Molecular weight, g/mol	Molecular structure	Solubility in water, mol/L	pK <sub>ow</sub>	pK <sub>a1</sub>	pK <sub>a2</sub>
171.15		0.041	0.02	2.58	14.44

### Preparation of nZVI and nanoscale Fe/Ni bimetallic and characterizations

nZVI particles prepared according to the method reported by Hwang et al. [23] were used in the experiments. nZVI synthesis was carried out under conditions of reductant delivery rate: 20 mL/min,  $[\text{BH}_4^-]$ : 358.5 mM and  $[\text{Fe}^{3+}]$ : 71.7 mM. The reduction reaction can be explained according to (R.3). The solution was filtered

by vacuum filtration to collect the resulting gray-black nZVI and then the formed particles were washed several times with ethanol, dried and stored in an anaerobic chamber.



A method given by Li et al. [13] was used to prepare a series of nFe/Ni bimetallic. For this purpose, firstly, 300 mL of ethanol and 2 g of nZVI were added to an Erlenmeyer flask. Then, 1 mL of NiCl<sub>2</sub>·6H<sub>2</sub>O solution prepared in 20 g/L ethanol was added to flask. The addition of NiCl<sub>2</sub> solution was adjusted by considering the desired Ni accumulation on nZVI, and mass balance calculations were made separately for Ni content of 1 wt%, 3.5 wt% and 10 wt%.

The concoction was agitated at a velocity of 300 revolutions per minute for a duration of 15 minutes, facilitating the adherence of Ni onto the nZVI substrate. Subsequent to Ni's adherence onto nZVI (R.4), the resultant Fe/Ni composites were segregated via magnetic means. In order to ascertain the coverage of ZVI particles by Ni, the concentration of Ni in the filtrate was quantified utilizing an Atomic Absorption Spectrometer (AAS). Conclusively, the Fe/Ni composites underwent a cleansing process with ethanol and were subjected to drying for a span of 2 hours at a temperature of 100°C.



The structural characteristics of nFe/Ni and the alterations in their chemical compositions pre and post-reaction were evaluated through the employment of a ZEISS Sigma 300 scanning electron microscope (SEM) (Cambridge, England) coupled with an energy-dispersive X-ray spectrometer (EDX) for analysis. Imagery of the specimens was captured at varied zoom levels, employing an operational voltage setting of 20 kV. The assessment of the surface area and the distribution of pore sizes within the samples was conducted using a Micromeritics Tristar II 3020, through the process of nitrogen adsorption and desorption techniques, with the surface area being deduced via the Brunauer-Emmett-Teller (BET) approach.

### **Experimental procedures**

Studies on the generation of H<sub>2</sub>O<sub>2</sub> and •OH radicals using the nFe/Ni catalyst were conducted at ambient conditions (22±2 °C) in a 500 mL beaker exposed to the open air. Throughout the chemical processes, atmospheric air was propelled into the beaker using an air sparger at a delivery rate of 150 L/hr. A motor-powered impeller (Heidolph RZR 2041), positioned at the beaker's base, was utilized to stir the solution at a speed of 300 revolutions per minute, ensuring a homogeneous dispersion of the bimetallic nanoparticles. Visual documentation of the experimental setup is provided in Supplementary Materials S1. The concentration of dissolved oxygen was monitored in real-time with a DO meter, which was adjusted to reach saturation at the experiment's inception. To thoroughly assess the pH's impact on the Fenton reaction, the initial pH of the solution was regulated to both 3 and 7 through the addition of 1 N H<sub>2</sub>SO<sub>4</sub> and NaOH, with manual adjustments made throughout the experiment. The ideal dosage of nFe/Ni was determined by conducting tests at both an initial MNZ concentration of 25 mg/L and at the aforementioned pH levels. The starting concentration of MNZ was set at a higher threshold to facilitate

the analytical detection limit via HPLC and to elucidate the mechanism behind MNZ removal. All experiments were replicated for accuracy.

### ***Analysis***

To assess the levels of H<sub>2</sub>O<sub>2</sub>, total Fe, Fe(II) and Fe(III), MNZ, and TOC, samples were collected at specific intervals. The H<sub>2</sub>O<sub>2</sub> content was measured using a UV-VIS spectrophotometer (PerkinElmer Lambda 365) at a wavelength of 385 nm employing potassium titanium oxalate as per reference [24], while the concentrations of total Fe and Fe(II) were quantified via the ferrozine method referenced in [25]. Samples were filtered through 0.22 µm disposable syringe filters. For the analysis of Fe(II), 1 mL of 3.6 M H<sub>2</sub>SO<sub>4</sub>, 1 mL of 4.9 mM Ferrozine solution, and 1 mL of acetate buffer were sequentially added to the samples before measurements were taken with a UV-spectrophotometer. The total concentration of Fe(III) in solution could be deduced by subtracting the Fe(II) concentration from the total dissolved iron content. Calibration curves for H<sub>2</sub>O<sub>2</sub>, ranging from 5-30 mg/L, were established, demonstrating a high correlation coefficient (0.999). The concentration of MNZ was determined through HPLC (Shimadzu) using an AllureBiPh column (5 µm, 150 × 4.6 mm) for 2 mL samples collected and filtered through a 0.22 µm membrane at predetermined times. The mobile phase, a mix of ammonium dihydrogen phosphate/acetonitrile (20:80, v/v), had a pH of 2.45 to 2.55. The volume and flow rate for the samples were set at 100 µL and 1.2 mL/min, respectively. MNZ detection was executed at 315 nm using a diode array detector, noting a retention time of 3.4 minutes. A calibration curve, drawn from five standards ranging between 20 and 100 mg/L, resulted in an R<sup>2</sup> value of approximately 0.998. TOC levels were gauged using a Shimadzu (TOC-VOPN) analyzer. LC-MS/MS (Shimadzu UFLC, AB 3200 Qtrap MS/MS) facilitated the identification of MNZ degradation products, examining an ion mass/charge ratio from 40/350 m/z. The AllureBiPh column (5 µm, 150x4.6 mm) was utilized with a mobile phase of 50:50 ultrapure water + 0.1% formic acid/acetonitrile + 0.1% formic acid, maintaining a flow rate of 0.4 mL/min and a column temperature of 40 °C, with the injection volume set at 100 µL.

## **RESULTS AND DISCUSSION**

### ***Fe/Ni characterization***

The morphologies of nFe/Ni at different Ni loading rates before and after the reaction at pH:3 and 7 were characterized by SEM and the elemental changes of nFe/Ni surface were analyzed by EDX. As shown in Supplementary Materials S2 (a,b,c), the raw nFe/Ni particles tend to accumulate because of the magnetic properties of the iron particle, it has an aggregation property. The particle diameter showed a distribution in the range of 40-80 nm. There were no remarkable changes in the morphologies of bimetallic particles synthesized at different Ni loading rates. However, as we expected, the element's content of nFe/Ni before reaction varied depending on Ni loading rate. For instance, Ni content was 1.30, 3.65, and 10.77 wt% corresponding to 1, 3.5, and 10 wt% of Ni loading rate, respectively.

After the reaction of pH:3, changes in surface morphologies showed that the spherical structure deteriorated independent of the nickel loading rate as shown in Supplementary Materials S3 (a,b,c). This may be due to Fe dissolution in acidic conditions and the formation of iron oxide by aeration. Combined with the SEM

images, the oxygen content increased in all bimetallic particles due to continuous aeration while the contents of Fe and Ni decreased. The slight variation in oxygen content according to Ni loading rate was observed. For example, the oxygen content was found to be 27.9, 23.1, and 20.3 wt% at 1, 3.5, and 10 wt% of Ni loading rate, respectively.

The shape of the nFe/Ni bimetallic particle obtained after the experiments carried out under pH:7 condition showed a different structure compared to that of pH:3, as seen in Supplementary Materials S4 (a,b,c). Much more agglomeration of particles was observed and core-shell structure related to iron oxide was seen as prominent. This is consistent with the study of Yamaguchi et al. [14] which showed that high pH (pH:8) triggered the formation of iron oxide/hydroxide. Moreover, the increases in C elements (16.73 wt% at 1 wt% of Ni loading rate) suggest that MNZ and its intermediates could be adsorbed onto the ZVI surface since more active sites resulted from the formation of iron/hydroxide were available for adsorption of contaminants. On the other hand, according to the BET analysis, the specific surface area of raw nFe/Ni and nFe/Ni after the reaction of pH:3 and 7 were found to be 40.77, 124, and 62.57 m<sup>2</sup>/g, respectively. Moreover, there was a remarkable increase in the BET surface area of the synthesized nFe/Ni bimetallic particles in the experiments carried out at pH:3. At low pH, the surface area of BET increased approximately 3 times, due to breaking from the surface. This situation was also related to the iron corrosion that appeared to occur from the SEM images (Supplementary Materials S3). After the reaction at pH:7, there was a slight increase in the BET surface area which may be related to the denser iron oxide layer covering the ZVI surface. Thus, the less active sites presented for nitrogen adsorption [14].

### ***The effect of Ni loading on profiles of Fe species, DO, H<sub>2</sub>O<sub>2</sub>, MNZ, and TOC***

#### ***The profiles of Fe species***

It is well known that the effect of pH was considered with two approaches. On one hand, Fenton oxidation of organic contaminants occurred faster at low pH thanks to the release of more Fe<sup>+2</sup> ions, resulting in more hydroxyl radicals (R.1). On the other hand, a passive film involving iron oxide/hydroxide formed on the iron surface may be responsible for removal of organic contaminants and their intermediate products [16]. Therefore, the influence of the second metal loading rate on profiles of Fe species, DO, H<sub>2</sub>O<sub>2</sub>, MNZ, and TOC was also examined at initial solution pH of 3 and 7. In order to find optimum pH, all experiments were employed 25 mg/L of MNZ and 0.1 g/L nFe/Ni. Fig 1(a) shows the results of the concentration of Fe<sup>+2</sup> against time for all nFe/Ni at different Ni loading rates at pH:3. Fe(II) was released into the solution within 30 min at all experiments. The iron elution of nFe/Ni also continuously and gradually raised in the presence of oxygen according to R(1). For 1 wt% of Ni loading rate, the Fe<sup>+2</sup> concentration was 10.66 mg/L within 1 hr while it reached about 15 mg/L at the end of the reaction time (2 hr). Considering high MNZ removal within 1 hr as discussed below, it was concluded that extending the reaction time under acidic conditions would not provide an advantage. The increasing Ni loading rate resulted in a slight decrease in iron elution after 1 hr as the dissolved Fe<sup>+2</sup> concentration was 10.66, 9.12, and 8.11 mg/L for 1, 3.5, and 10 wt% of Ni loading rate, respectively. It is evident that higher Ni loading could not provide protection against iron corrosion under acidic conditions. However, iron elution is of great significance in the stability and reuse of catalysts as well as in-situ generation of H<sub>2</sub>O<sub>2</sub> and •OH radicals. Our results also show that dissolved Fe (II) at all Ni loading rates was in the range of 10-20% of 0.1 g/L nFe/Ni dosage. Several studies

on heterogeneous Fenton reactions by using zero-valent iron-based particles determined the iron elution to different extents. For example, Harada et al. [9] determined that complete dissolution occurred after 1440 minutes in experiments performed at an initial ZVI concentration of 0.9 mM and pH:3. Shimizu et al. [26] stated that the  $\text{Fe}^{2+}$  concentration reached up to 1000 mg/L after 100 minutes and this value would be sufficient to continue the Fenton reaction. Takayanagi et al. [27] and Fujioka et al. [16] also determined Fe dissolution as being about 20% and 90% of the initial dosage, respectively. Furthermore, the analysis results belonging to the  $\text{Fe}^{3+}$  show that the concentration  $\text{Fe}^{3+}$  was very low hence it was not shown in the graphs. These results concluded that the reduction of  $\text{Fe}^{3+}$  or the regeneration of  $\text{Fe}^{2+}$  formed in the process. On the other hand, no elution of Fe ions occurred at pH:7 as the concentration of  $\text{Fe}^{2+}$  was found as low as 0.1 mg/L and remained approximately constant. Therefore the effect of Ni loading rate on Fe(II) concentration at pH:7 was negligible as depicted in Fig 1(b). This implies that the surface of nFe/Ni is covered by the passive iron hydroxide layer because of the process of hydrolysis of iron ions. This result was also supported by EDX and BET analysis at pH:7 condition, which revealed the formation of iron hydroxide.

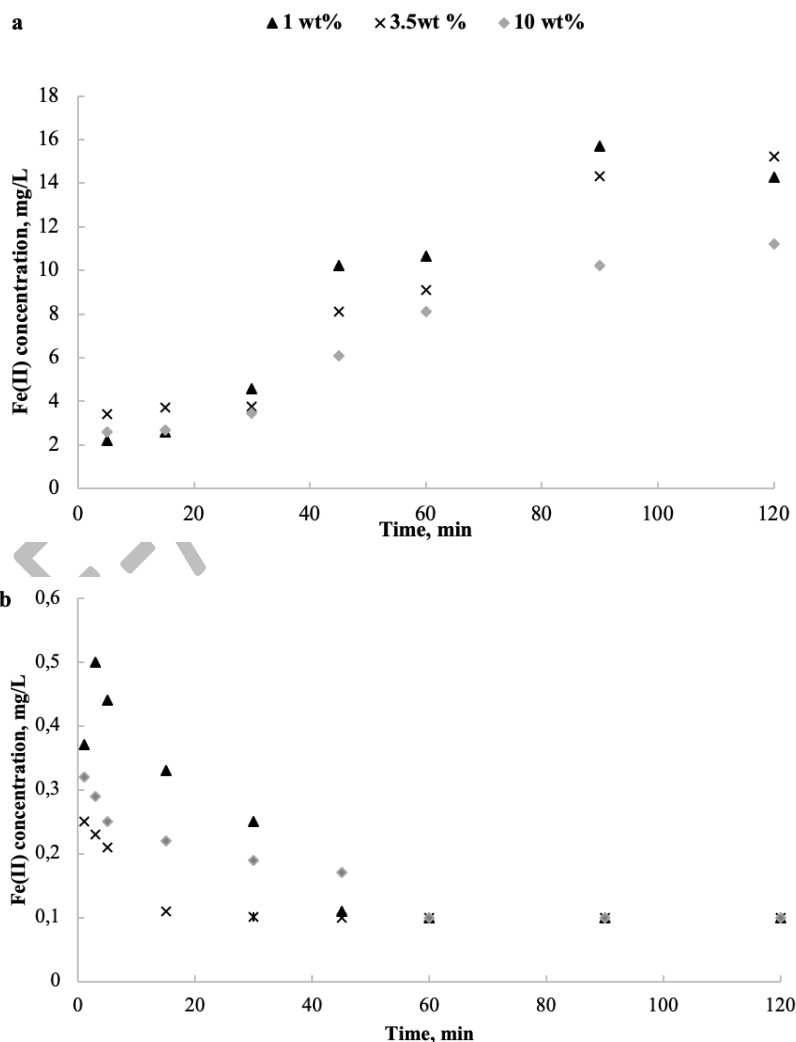
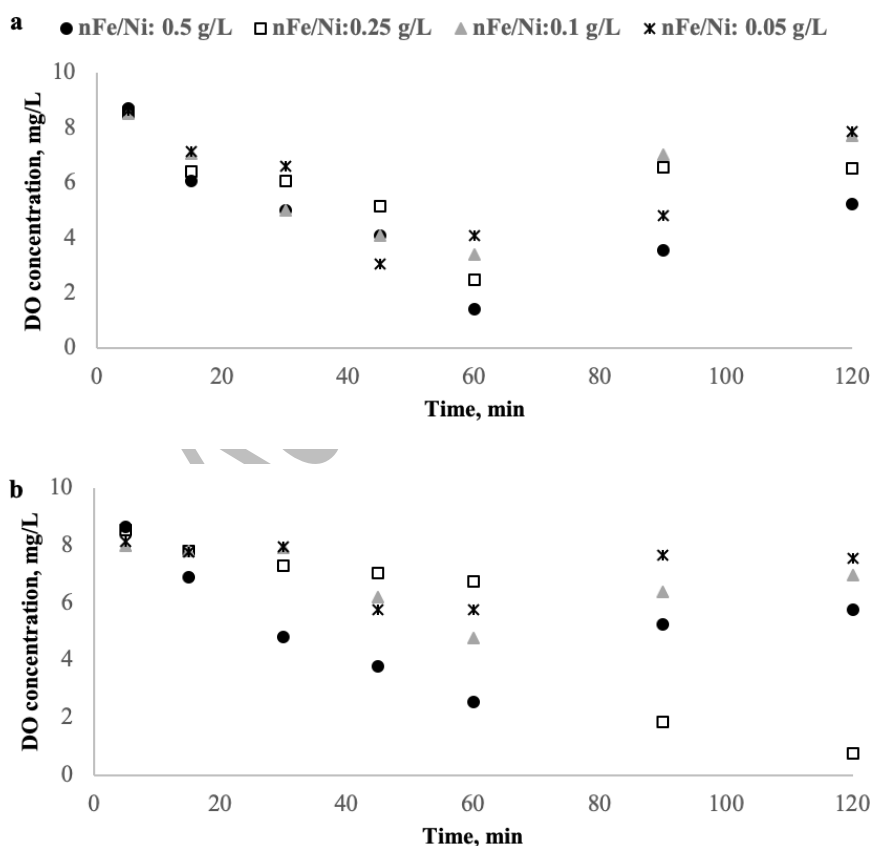


Fig 1 Fe(II) concentration during the reaction at pH:3 (a) and pH:7 (b) (for 25 mg/L of MNZ and 0.1 g/L nFe/Ni)

The profiles of DO and  $\text{H}_2\text{O}_2$

Dissolved oxygen concentration affects the generation of  $\cdot\text{OH}$  radical as well as the formation of an iron oxide/hydroxide layer [9, 26]. The experiments were conducted solely at pH 3, with varying nFe/Ni dosages for all Ni loading rates since the results for DO and  $\text{H}_2\text{O}_2$  obtained at pH 7 showed that the DO concentration remained constant while the  $\text{H}_2\text{O}_2$  concentration was close to zero.

Fig 2 shows the change of DO concentration at different Ni loading rates. The DO concentration changed over the course of the reaction time, even though it was at saturation at the beginning of the experiments. This could be related to the balance between dissolution and consumption of DO by the nFe/Ni bimetallic surface according to R(4) and iron oxide layer formation. By considering the  $\text{H}_2\text{O}_2$  detection as depicted in Fig 3 (a,b,c), DO is remarkably used to generate in-situ  $\text{H}_2\text{O}_2$  as well as to form an iron oxide/hydroxide layer. It also implies that DO consumption was considerably fast even if the oxygen was continuously sparged into the solution. As shown in Fig 2, the concentration of DO decreased from 8.72 mg/L to 1.41 mg/L within 1 hr and then reached to 5.24 mg/L at dosage of 0.5 g/L for 1 wt%. For, 3.5 wt% and 10 wt% of Ni loading rate, DO was found to be 2.57 and 5.17 mg/L within the same reaction time and complete recovery of DO was not detected during the reaction time.





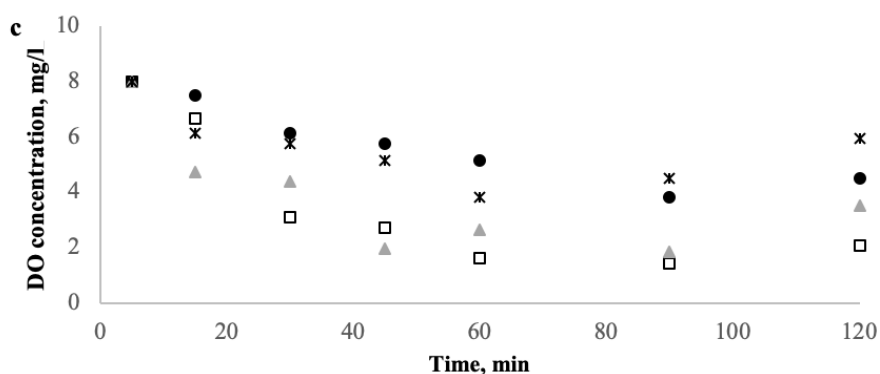


**Fig 2** Dissolved oxygen concentration during the reaction at pH:3, 25 mg/L initial MNZ concentration, different Ni loading rate and nFe/Ni dosages (1 wt% Ni (a), 3.5 wt% Ni (b), 10 wt% Ni (c))

It is also clearly seen from Fig 2(a) that the DO concentration was more affected by nFe/Ni dosage than the Ni loading rate. The increase in Fe/Ni dosages led to a greater decrease in DO. For instance, the minimum DO concentrations reached for the nFe/Ni dosages of 0.5 and 0.05 g/L within 1 hr were 1.41 and 4.1 mg/L, respectively. High nFe/Ni dose increases the number of active sites on the bimetallic surface and the release of Fe(II), facilitating the reactions with DO and the formation of H<sub>2</sub>O<sub>2</sub>. Similar to the present results, Feitz et al. [28] found that nZVI particles with a large specific surface area rapidly reacted with H<sub>2</sub>O<sub>2</sub> and DO to generate Fe(II) and iron oxides/hydroxides during the initial stage. Takayanagi et al. [27] also reported that oxygen consumption accelerated by increasing ZVI dosage because of the much higher iron oxides/hydroxides formation.

Fig 3 (a,b,c) illustrates the concentration of H<sub>2</sub>O<sub>2</sub> employing the reaction with different nFe/Ni dosages at 1 wt%, 3.5 wt%, and 10 wt% of Ni loading rate, respectively. It is clear that the increase in nFe/Ni dosage caused more generation of H<sub>2</sub>O<sub>2</sub> at all Ni loading rates especially for 3.5 and 10 wt% of Ni loading rate. For instance, an increase of more than 10 times for H<sub>2</sub>O<sub>2</sub> concentration was determined by increasing nFe/Ni dosage from 0.05 g/L to 0.5 g/L at 10 wt% of Ni loading rate. This implies that more active sites with a high dosage of nFe/Ni could react with dissolved oxygen to form H<sub>2</sub>O<sub>2</sub>. In contrast to results from DO profiles at different nFe/Ni dosages, a remarkable effect of Ni loading rate on the in-situ generation of H<sub>2</sub>O<sub>2</sub> was also observed. The maximum H<sub>2</sub>O<sub>2</sub> concentration was found as 3.29 mg/L, 11.97 mg/L, and 19 mg/L at Ni loading rates of 1, 3.5, and 10 wt%, respectively. In many studies the H<sub>2</sub>O<sub>2</sub> concentration could not be analyzed because the H<sub>2</sub>O<sub>2</sub> formed was quickly consumed to form •OH radicals according to R(1) [9, 14, 26]. Therefore, the formation of •OH radicals was confirmed by adding a radical scavenger to the solution or by measuring the •OH radical concentration. However, Liu et al. [24] investigated the degradation of sulfamethoxazole by Zn-Fe-CNTs via a Fenton-like process and found that the H<sub>2</sub>O<sub>2</sub> concentration at pH: 1.5 and 7 within 10 min was 5.26 mg/L and 22.2 mg/L, respectively. Karim et al. [29] also studied the degradation of 17-ethinylestradiol with nano-zerovalent iron at different dissolved oxygen levels and different pHs and analyzed the H<sub>2</sub>O<sub>2</sub> concentration as 8 μM. Hence, it is more important to confirm the formation of •OH radical by considering the MNZ and TOC removals than to detect the concentration of H<sub>2</sub>O<sub>2</sub> as discussed in Section 3.2.3.

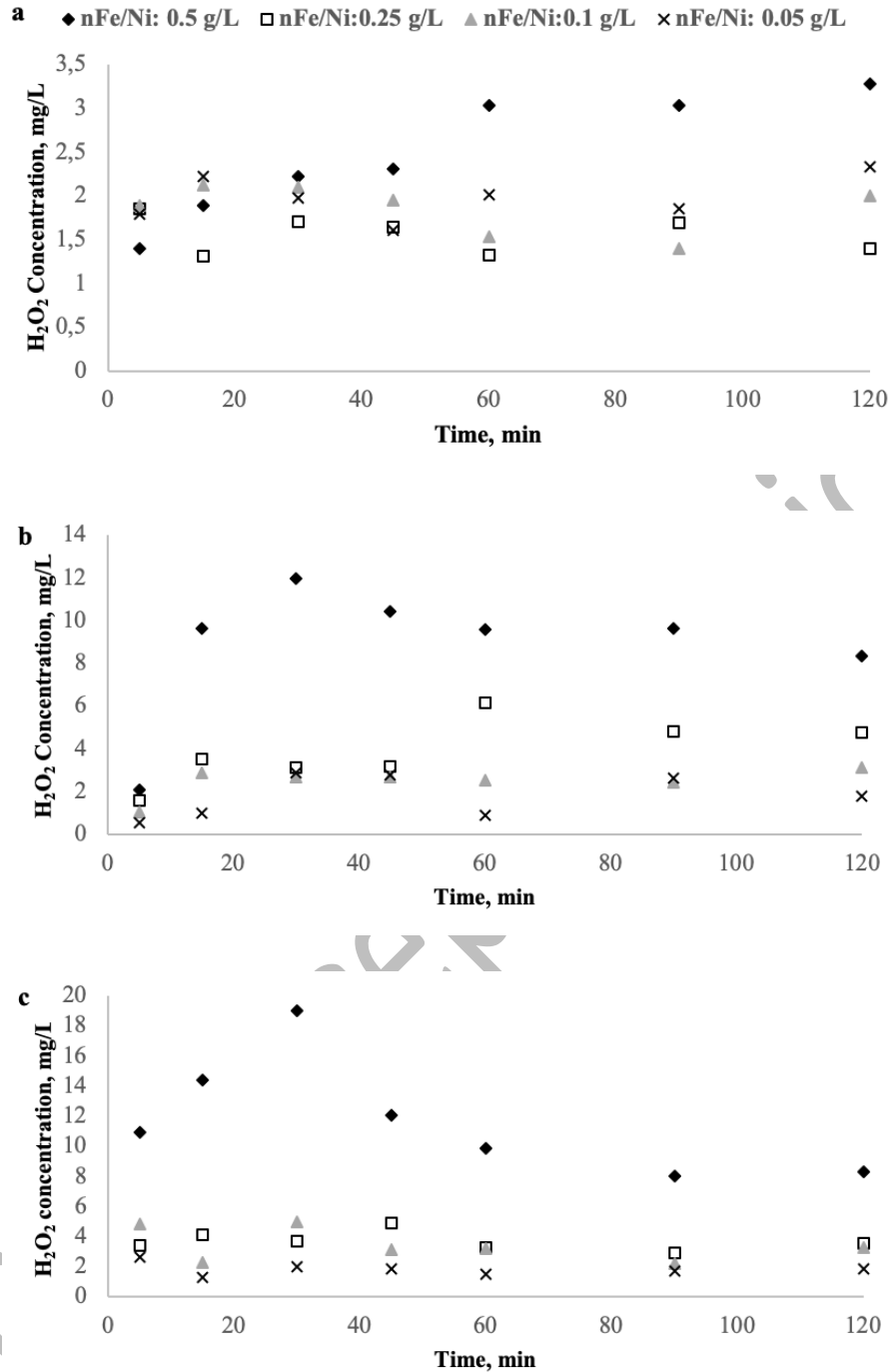


**Fig 3 H<sub>2</sub>O<sub>2</sub> concentration during the reaction at pH:3, 25 mg/L initial MNZ concentration, different Ni loading rate and nFe/Ni dosages (1 wt% Ni (a), 3.5 wt% Ni (b), 10 wt% Ni (c))**

*MNZ and TOC removal and insight into removal mechanism by nFe/Ni*

The effect of Ni loading rate on the Fenton-like process was also evaluated with MNZ and TOC removal since the degradation of organic compounds is generally inhibited by the hydroxyl radicals which are rapidly scavenged by Fe<sup>2+</sup>, H<sub>2</sub>O<sub>2</sub>, •OH radical, HO<sub>2</sub><sup>-</sup> in Fenton process [17, 26]. According to the leaching experiment of Fe ions (Fig 1), a significant effect of Ni loading rate on the dissolution of nFe/Ni was not observed. However, the concentration of H<sub>2</sub>O<sub>2</sub> was strongly related to the change in the Ni loading rate. The removal of MNZ and

TOC was mainly controlled by the reaction between MNZ oxidation and the production of  $\bullet\text{OH}$  radical, which was the main oxidant in the oxidation process. Fig 4(a,b) shows the MNZ and TOC removals for 1 wt% Ni loading rate at pH:3 and 7, respectively. MNZ removal was found approximately 99% with all nFe/Ni dosages except for the dosage of 0.05 g/L at both pH (Fig 4(a,b)). Although the high removal efficiency of MNZ was achieved at pH:7, the removal mechanism was differed greatly from that of pH:3. By considering little iron elution at pH:7 mentioned above it may be concluded that the nFe/Ni surface could mainly contribute to the adsorption of MNZ. Moreover, it is clear that TOC removal (between 5% and 20%) at pH:7 shows that the removal mechanism of MNZ depends on the adsorption process. It is also apparent from Fig 4(a), further increase in catalyst dosage led to a significant increase in TOC removal at pH:3. When the catalyst dosage was increased from 0.1 g/L to 0.5 g/L, the efficiency of TOC removal increased significantly from 28% to 45% at the end of the reaction. Yang et al. [30] and Pourabadeh et al. [3] found that increasing the amount of adsorbent led to higher dye and drug adsorption efficiency due to the increase in the number of active sites and adsorbent surface.

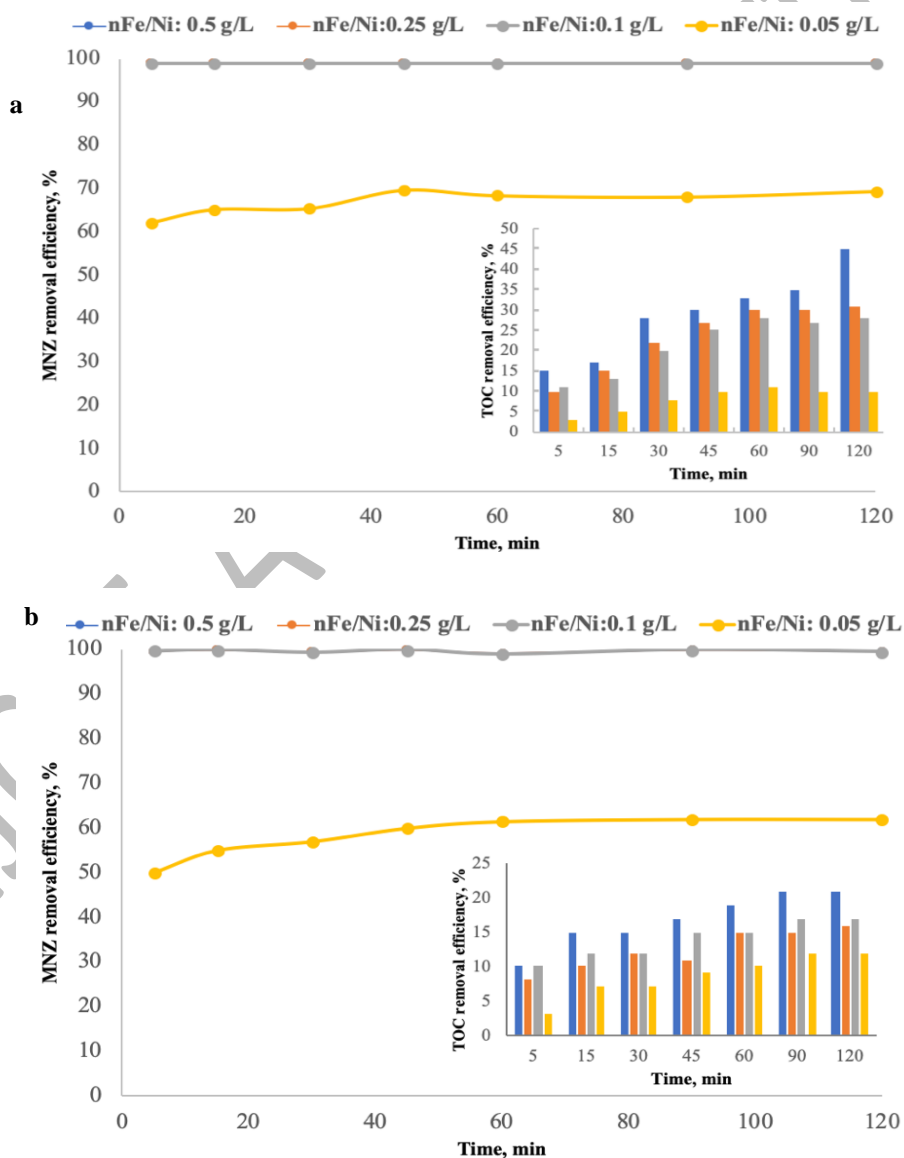


Fig 4 MNZ and TOC removal at 1 wt% Ni loading rate, 25 mg/L initial MNZ concentration and different nFe/Ni dosages (pH:3(a) and pH:7 (b))

Fig 5(a,b) shows the results belonging to MNZ and TOC removal at 3.5 wt% Ni loading rate at pH:3 and 7, respectively. A clear dependency of MNZ and TOC removal on nFe/Ni dosage was determined. At pH:3, the MNZ removal reached 99% and 57% by 0.1 g/L and 0.05 g/L of nFe/Ni within 1 hr, respectively. In contrast to high MNZ removal, only 12% TOC removal was achieved by 0.1 g/L of nFe/Ni while the maximum TOC removal was found as 28% by 0.5 g/L of nFe/Ni. As depicted in Fig 5(b), a remarkable reduction in MNZ removal was also observed with low nFe/Ni dosage at pH:7. The MNZ removal efficiency within 120 min was 71% and 18% with a dosage of 0.1 g/L and 0.05 g/L, respectively. Similar to findings of 1 wt% Ni loading rate, TOC removal was negligible at pH:7 because iron oxide/hydroxide would form a passivation film layer on the nFe/Ni surface under alkaline and neutral conditions, inhibiting iron corrosion and react with organic contaminants. According to Luo et al. [31], the degradation efficiency of MNZ using B-FeOOH decreased as the initial pH increased from 3 to 9. This was attributed to the low  $\bullet\text{OH}$  radical via  $\text{H}_2\text{O}_2$  activation. Compared to 1 wt% Ni loading rate, the lower TOC removal was obtained at 3.5 wt% of Ni loading rate at pH:3. Based on the leaching experiment, Fe ions dissolved slightly more at 3.5 wt% nFe/Ni than that at 1 wt% of Ni loading rate. Hence, it shows that another parameter can play a key role to inhibit the further oxidizing ability of MNZ. The reason for decreased TOC removal might be more generation of  $\text{H}_2\text{O}_2$  which can employ as a scavenger of  $\bullet\text{OH}$  radical that inhibit the further degradation of organic compounds [32-34]. This was also confirmed at the experiments of 10 wt% Ni loading rate in which excess  $\text{H}_2\text{O}_2$  was obtained as discussed in Section 3.2.2 and decreases in MNZ and TOC removal were determined at pH:3. Figure 6(a) shows that after 1 hr of reaction, MNZ removal efficiency was approximately 93% and 50% with 0.1 g/L and 0.05 g/L of nFe/Ni dosage, respectively. As can be seen in Fig 6(b), similar behavior was observed in TOC removal which decreased from 20% to 10% with the same nFe/Ni dosage. Herein it is important to note that the optimal  $\text{H}_2\text{O}_2/\text{nFe/Ni}$  mass ratio plays a crucial role in the production of  $\bullet\text{OH}$  radicals (R.5). Deng et al. [33] stated that the mass ratio of  $\text{H}_2\text{O}_2/\text{nZVI}$  can affect the scavenging of  $\bullet\text{OH}$  radicals, which can retard the degradation of sulfamethazine in the Fenton-like process. On the other hand, the increasing Ni loading could not improve the MNZ removal at pH:7 since the removal mechanism mainly depended on surface adsorption. At neutral pH, it is also apparent that nFe/Ni dosage has a more remarkable effect on the removal of MNZ rather than the Ni loading rate. It can relate to the high surface area provided by using high dosage in adsorption process. Additionally, a significant TOC removal was not achieved, consistent with the results obtained at 1 wt% and 3.5 wt% Ni loading rate.



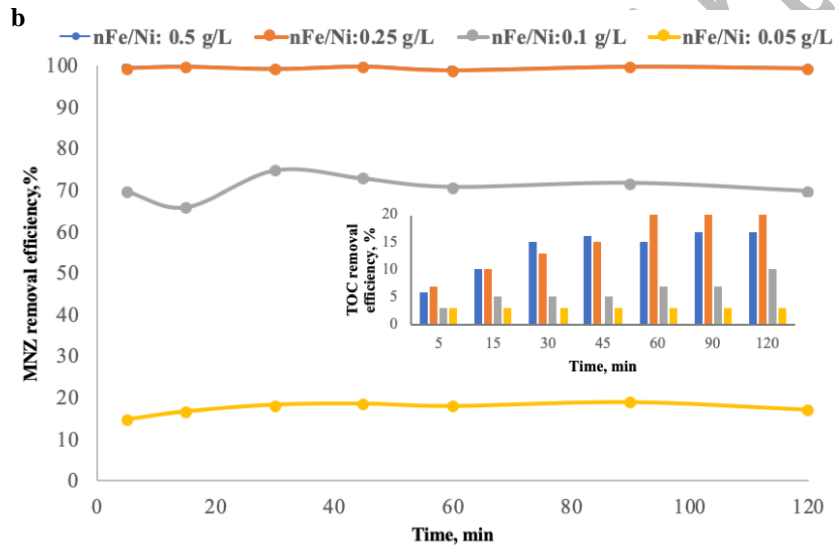
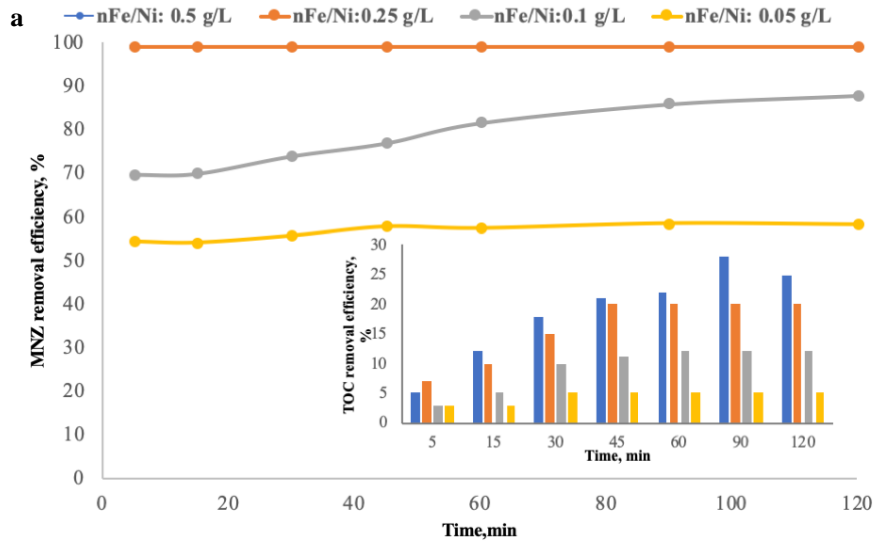


Fig 5 MNZ and TOC removal at 3.5 wt% Ni loading rate, 25 mg/L initial MNZ concentration and different nFe/Ni dosages (pH:3(a) and pH:7 (b))

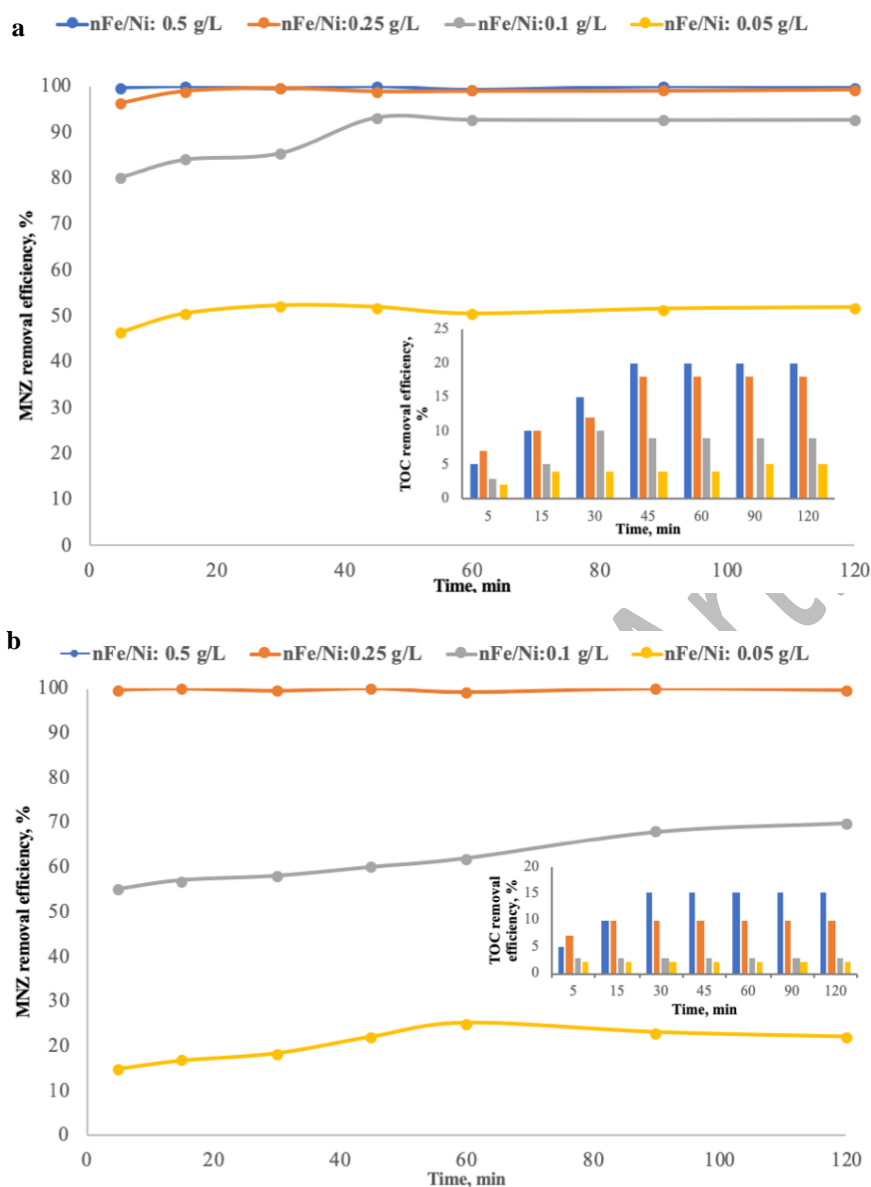
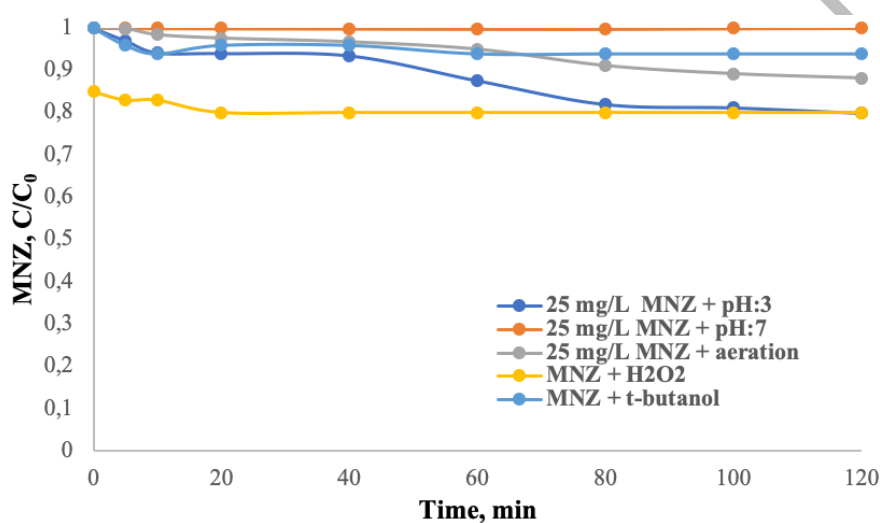


Fig 6 MNZ and TOC removal at 10 wt% Ni loading rate, 25 mg/L initial MNZ concentration and different nFe/Ni dosages (pH:3(a) and pH:7 (b))

On the other hand, to evaluate the performance of the Fenton-like process for MNZ and TOC removal, several experiments were conducted to control potential MNZ losses during the reactions. These control experiments are as follows: only H<sub>2</sub>O<sub>2</sub> treatment, only aeration, and only with nFe/Ni bimetallic particles at initial pH values with 25 mg/L of MNZ. Furthermore, to confirm the impact of OH radicals on MNZ removal and their presence, 200 mM t-butanol was added as a scavenger. Figure 7 shows the results from blank experiments. It was noteworthy that no significant decrease in MNZ concentration was observed in all other blank experiments, except for the experiments with pH: 3 solution and H<sub>2</sub>O<sub>2</sub> alone, where MNZ removal efficiency was 12% and 23%, respectively. The inability to remove MNZ with only 0.1 g/L nFe/Ni within 120 minutes at pH 3 confirms that MNZ could not adsorb at this pH. In contrast, employing the reaction at pH:7 without the addition of nFe/Ni, the efficiency of MNZ removal was approximately 5%, indicating a strong reliance on the adsorption process for MNZ elimination. Conversely, to gain deeper insight into the mechanism of removal at pH 3, two distinct TOC

measurements were conducted. Initially, TOC levels in the aqueous samples highlighted the MNZ removal process, as depicted in the graphical data. Subsequently, after the completion of the reaction, the precipitated and non-soluble nFe/Ni was filtered, dried for 3 hours at 30 °C, and then acidified using 9.4 mM H<sub>2</sub>SO<sub>4</sub> before performing TOC analysis. These results were intended to reflect the concentration of MNZ and its degradation products in the presence of nFe/Ni. However, the TOC values were unobtainable through this method, corroborating the inability of MNZ and its by-products to adsorption to the nFe/Ni surfaces at pH 3. Furthermore, Fig 7 illustrates that the excessive inclusion of t-butanol significantly impeded the MNZ removal process. This observation aligns with other research findings related to the degradation of substances such as chlorpheniramine, diclofenac, sulfadiazine, and sulfamethazine through ZVI in a Fenton-like reaction [24, 32, 35, 36].



**Fig 7 Results of blank experiments performed under different conditions for MNZ removal**

TOC conversion is important in removing pollutants to eliminate environmental hazards caused by wastewater discharge. In our study, TOC removal was low in all experiments compared to the complete removal of MNZ. Formation of poorly degradable intermediates can result in low TOC removal. Several studies have achieved complete removal of MNZ with varying degrees of degradation. For example, Nasseh et al. [22] utilised a FeNi<sub>3</sub>/SiO<sub>2</sub> magnetic nanocomposite to oxidize MNZ in a heterogeneous Fenton-like process. They were able to achieve a maximum removal of 59% of TOC. In another study, total MNZ degradation in the electro-Fenton process was investigated and 40% mineralization was achieved in electrolysis with 0.1 mM iron ions for 20 minutes and 135 minutes respectively at pH:3 and 0.07 mA/cm<sup>2</sup> [37]. Furthermore, a study using a solar photoelectron-Fenton process detected a slight improvement in biodegradation as a result of the recalcification of metronidazole by-products. [22].

Since approximately 45%, 27% and 20% of the initial TOC was removed after 120 min at Ni loading of 1 wt%, 3.5 wt% and 10 wt%, respectively, intermediates of MNZ were identified by LC/MS-MS technique and mineralization process of MNZ by nFe/Ni bimetallic was explained. The batch experiments were conducted with 0.1 g/L nFe/Ni and 25 mg/L MNZ at pH:3. Figure 8 presents a schematic representation of the proposed degradation products for MNZ. A variety of identified products was shown in Supplementary Materials S5. They include m/z 128 (2-methyl-4-nitroimidazole or 2-methyl-5-nitroimidazole), 114 (4-nitroimidazole), 172 (ethanol)

and 82 (2-methyl-1H-imidazole) which proves the occurrence of MNZ mineralization with variable degrees at all nFe/Ni loading rate. This is well consistent with the findings of Yan et al. [37] and Chen et al. [38] who also observed similar intermediates belonging to the MNZ by a modified electrochemical Fenton and adsorption process, respectively. The reduction of the nitroso group of MNZ to the amino group resulted in the formation of 2-methyl-5-nitroimidazole, -(2-hydroxyethyl)-2-methyl-5-aminoimidazole intermediates. The degradation pathways for MNZ are carried out by nitro reduction and N-denitration [38]. Then, with the continuous formation of the  $\bullet\text{OH}$  radicals, the products formed were converted to 2-methyl-1H-imidazol-5-ol by dealkalization and decarboxylation reactions, and in the last stage, smaller molecules were formed by the separation of the ring in the MNZ structure [31].

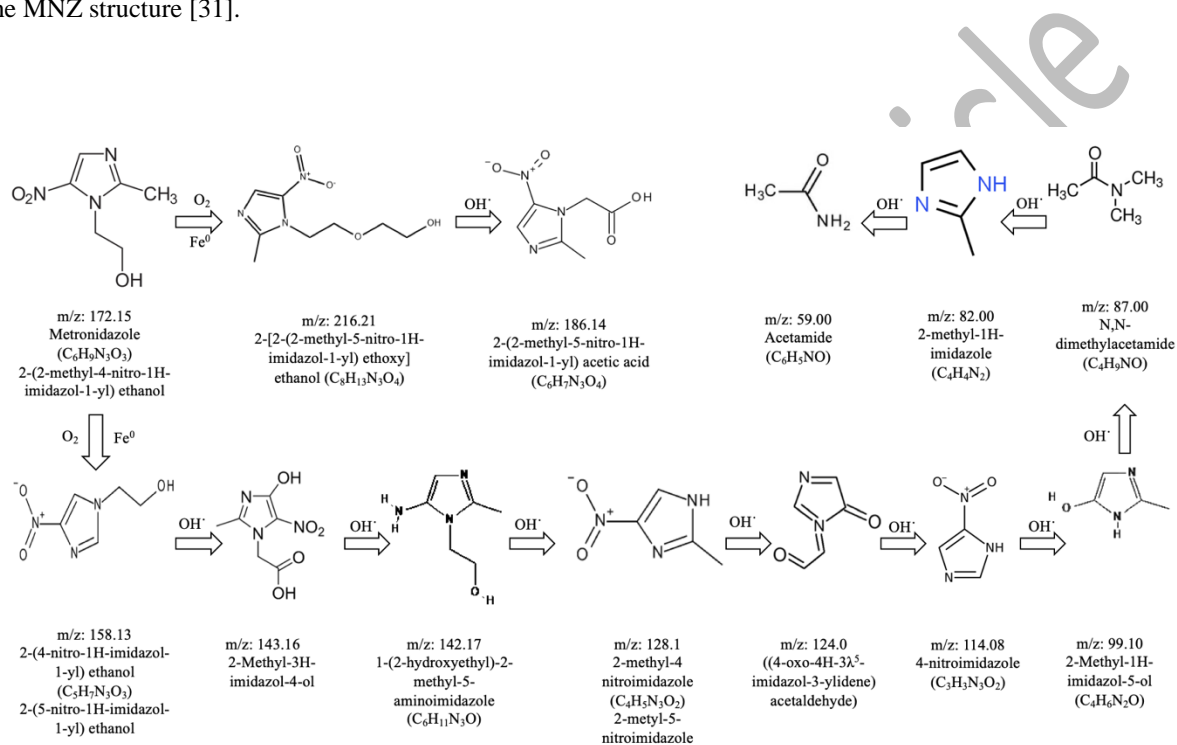


**Fig 8 Degradation intermediates of MNZ with 0.1 g/L nFe/Ni (for 25 mg/L initial MNZ concentration and pH:3)**

## CONCLUSIONS

Compared to previous studies focusing on second metal loading, in this study the addition of Ni to zero-valent iron significantly affected the in-situ generation of  $\text{H}_2\text{O}_2$ . Higher Ni loading on nFe/Ni was found to enhance the generation of  $\text{H}_2\text{O}_2$  at acidic pH and increase the adsorption capability of nFe/Ni at neutral pH. However, it was observed that this did not stimulate the generation of  $\bullet\text{OH}$  radicals due to the scavenging effect of excessive  $\text{H}_2\text{O}_2$ . Increasing the nickel loading ratio from 1 wt% to 10 wt% resulted in a six-fold increase in the maximum measured  $\text{H}_2\text{O}_2$  concentration, from 3.29 mg/L to 19 mg/L. Besides the Ni loading rate, nFe/Ni dosage also increased the amount of  $\text{H}_2\text{O}_2$  formation, and for a 10 wt% Ni loading rate, a 10-fold increase in nFe/Ni dosage increased the  $\text{H}_2\text{O}_2$  concentration more than 10 times. MNZ can be completely removed within 1 hr using nFe/Ni 0.1 g/L synthesized with a 1 wt% Ni loading rate and an initial MNZ concentration of 25 mg/L at pH 3 while only 45% TOC was removed after 2 hr. In addition, possible degradation products have been proposed considering the intermediates determined by LC/MS-MS. The conversion of MNZ to fragments with different molar masses



indicated that the degradation of MNZ occurred at varying degrees. Almost complete degradation of MNZ revealed that nFe/Ni particles have excellent potential for MNZ degradation.

## ACKNOWLEDGEMENTS

The significant part of this paper includes the Master Thesis data of Ecehan Şener. This research was supported by a grant from FUBAP with a project number of MF 20.15.

## AUTHOR CONTRIBUTIONS

All authors performed the analysis, data collection, and interpretation of results and contributed to the study's conception and design. All authors read and approved the final manuscript.

## STATEMENTS AND DECLARATIONS

There are no conflicts of interest in this research.

## REFERENCES

- [1] Keenan C.R., Sedlak D.L., [Factors Affecting the Yield of Oxidants from the Reaction of Nanoparticulate Zero-Valent Iron and Oxygen](#), *Environ. Sci. Technol.*, **42**(4): 1262-1267 (2008).
- [2] Cai L., Lin C., Yang N., Huang Z., Miao S., Chen X., Pan J., Rao P., Liu S., [Preparation And Characterization of Nanoparticles Made from Co-Incubation of SOD and Glucose](#), *Nanomaterials*, **7**(12): 458 (2017).
- [3] Pourabadeha A., Baharinikoob L., Shojaei S., Mehdizadehd B., Davoodabadi Farahani M., Shojaei S., [Experimental Design and Modelling of Removal of Dyes Using Nano-Zero-Valent Iron: A Simultaneous Model](#), *Int. J. Environ. Anal. Chem.*, **100**(15): 1707–1719 (2020).
- [4] Mirzaei A., Chen Z., Haghghat F., Yerushalmi L., [Removal of Pharmaceuticals from Water by Homo/Heterogeneous Fenton-Type Processes-A Review](#), *Chemosphere*, **174**: 665-688 (2017).
- [5] Yang Z., Zhang X., Pu S., Ni R., Lin Y., Liu Y., [Novel Fenton-Like System \(Mg/Fe-O<sub>2</sub>\) for Degradation of 4-Chlorophenol](#), *Environ. Pollut.*, **250**: 906-913 (2019).
- [6] Zhao J., Zhang Y., Quan X., Chen S., [Enhanced Oxidation Of 4-Chlorophenol Using Sulfate Radicals Generated from Zero-Valent Iron and Peroxydisulfate at Ambient Temperature](#), *Sep. Purif. Technol.*, **71**(3): 302-307 (2010).
- [7] Wang F., Yu X., Ge M., Wu S., Guan J., Tang J., Wu X., Ritchie R.O., [Facile Self-Assembly Synthesis of Γ-Fe<sub>2</sub>O<sub>3</sub>/Graphene Oxide for Enhanced Photo-Fenton Reaction](#), *Environ. Pollut.*, **248**: 229-237 (2019).

- [8] Yu X., Zhou M., Ren G., Ma L., [A Novel Dual Gas Diffusion Electrodes System for Efficient Hydrogen Peroxide Generation Used in Electro-Fenton](#), *Chem. Eng. J.*, **263**: 92-100 (2015).
- [9] Harada T., Yatagai M., Kawase Y., [Hydroxyl Radical Generation Linked with Iron Dissolution and Dissolved Oxygen Consumption in Zero-Valent Iron Wastewater Treatment Process](#), *Chem. Eng. J.*, **303**: 611-620 (2016).
- [10] Ezzatahmedi N., Millar J.G., Ayoko G.A., Zhu J., Zhu R., Liang X., He H., Xi Y., [Degradation of 2,4-Dichlorophenol Using Palygorskite-Supported Bimetallic Fe/Ni Nanocomposite as A Heterogeneous Catalyst](#), *Appl. Clay Sci.*, **168**: 276-286 (2019).
- [11] Liu J., Du Y., Sun W., Chang Q., Peng C., [Preparation of New Adsorbent-Supported Fe/Ni Particles for The Removal of Crystal Violet and Methylene Blue by A Heterogeneous Fenton-Like Reaction](#), *RSC Adv.*, **9**: 22513-22522 (2019).
- [12] Hussain S., Aneggi E., Goi D., Trovarelli A., [Bimetallic Cu/Fe Catalysts for Ibuprofen Mineralization](#), *Catalysts*, **11**: 1383 (2021).
- [13] Li Y., Li X., Han D., Huang W., Yang C., [New Insights Into The Role of Ni Loading on The Surface Structure and The Reactivity of nZVI Toward Tetrabromo- and Tetrachlorobisphenol A](#), *Chem. Eng. J.*, **311**: 173-182 (2017).
- [14] Yamaguchi R., Kurosu S., Suzuki M., Kawase Y., [Hydroxyl Radical Generation by Zero Valent Iron/Cu \(ZVI/Cu\) Bimetallic Catalyst in Wastewater Treatment: Heterogeneous Fenton/Fenton-Like Reactions by Fenton Reagents Formed In-Situ Under Oxidic Conditions](#), *Chem. Eng. J.*, **334**: 1537-1549 (2018).
- [15] Xiong Z., Lai B., Yang P., Zhou Y., Wang J., Fang S., [Comparative Study on The Reactivity of Fe/Cu Bimetallic Particles and Zero Valent Iron \(ZVI\) Under Different Conditions of N<sub>2</sub>, Air or Without Aeration](#), *J. Hazard. Mater.*, **297**: 261-268 (2015).
- [16] Fujioka N., Suzuki M., Kurosu S., Kawase Y., [Linkage of Iron Elution and Dissolved Oxygen Consumption with Removal of Organic Pollutants by Nanoscale Zero-Valent Iron: Effects of pH on Iron Dissolution and Formation of Iron Oxide/Hydroxide Layer](#), *Chemosphere*, **144**: 1738-1746 (2016).
- [17] Li R., Gao Y., Jin X., Chen Z., Megharaj M., Naidu R., [Fenton-Like Oxidation of 2,4-DCP in Aqueous Solution Using Iron-Based Nanoparticles as The Heterogeneous Catalyst](#), *J. Colloid Interface Sci.*, **438**: 87-93 (2015).
- [18] Marcelo C.R., Lopes R.P., Cruz J.C., Nascimento M.A., Silva A.A., Lima C.F., [Evaluation of Different Parameters on The Acetamiprid Degradation by Bimetallic Fe/Ni Nanoparticles](#), *Sep. Purif. Technol.*, **171**: 256-262 (2016).
- [19] Xie Z., Wang C., Yin L., [Nickel-Assisted Iron Oxide Catalysts for The Enhanced Degradation of Refractory DDT in Heterogeneous Fenton-Like System](#), *J. Catal.*, **353**: 11-18 (2017).
- [20] Sun Y., Yang Z., Tian P., Sheng Y., Xu J., Han Y.F., [Oxidative Degradation of Nitrobenzene by A Fenton-Like Reaction with Fe-Cu Bimetallic Catalysts](#), *Appl. Catal., B*, **244**: 1-10 (2019).

- [21] Wang J., Liu C., Li J., Luo R., Hu X., Sun X., Shen J., Han W., Wang L., [In-Situ Incorporation of Iron-Copper Bimetallic Particles Inelectrospun Carbon Nanofibers as An Efficient Fenton Catalyst](#), *Appl. Catal., B*, **207**: 316-325 (2017).
- [22] Nasseh N., Taghavi L., Barikbin B., Nasserri M.A., Allahresani A., [Feni<sub>3</sub>/SiO<sub>2</sub> Magnetic Nanocomposite as An Efficient and Recyclable Heterogeneous Fenton-Like Catalyst for The Oxidation of Metronidazole in Neutral Environments: Adsorption and Degradation Studies](#), *Composites, Part B*, **166**: 328-340 (2019).
- [23] Hwang Y.H., Kim D.G., Shin H.S., [Mechanism Study of Nitrate Reduction by Nano Zero Valent Iron](#), *J. Hazard. Mater.*, **185(2-3)**: 1513-1521 (2011).
- [24] Liu Y., Fan Q., Wang J., [Zn-Fe-CNTs Catalytic In Situ Generation of H<sub>2</sub>O<sub>2</sub> for Fenton-Like Degradation of Sulfamethoxazole](#), *J. Hazard. Mater.*, **342**: 166-176 (2018).
- [25] Stookey L.L., [Ferrozine-A New Spectrofotometric Reagent Iron](#), *Anal. Chem.*, **42**: 779-781 (1970).
- [26] Shimizu A., Tokumura M., Nakajima K., Kawase Y., [Phenol Removal Using Zero-Valent Iron Powder in The Presence of Dissolved Oxygen: Roles of Decomposition by The Fenton Reaction and Adsorption/Precipitation](#), *J. Hazard. Mater.*, **201-202**: 60-67 (2012).
- [27] Takayanagi A., Kobayashi M., Kawase Y., [Removal of Anionic Surfactant Sodium Dodecyl Benzene Sulfonate \(SDBS\) from Wastewaters by Zero Valent Iron \(ZVI\): Predominant Removal Mechanism for Effective SDBS Removal](#), *Environ. Sci. Pollut. Res.*, **24**: 8087-8097 (2017).
- [28] Feitz A.J., Joo S.H., Guan J., Sun Q., Sedlak D.L., Waite T.D., [Oxidative Transformation of Contaminants Using Colloidal Zero Valent-Iron](#), *Colloids Surf., A*, **265**: 88-94 (2005).
- [29] Karim S., Bae S., Greenwood D., Hanna K., Singhal N., [Degradation of 17 \$\alpha\$ -Ethinylestradiol by Nano Zero Valent Iron Under Different pH and Dissolved Oxygen Levels](#), *Water Res.*, **125**: 32-41 (2017).
- [30] Yang J., Shojaei S., Shojaei S., [Removal of Drug and Dye from Aqueous Solutions by Graphene Oxide: Adsorption Studies and Chemometrics Methods](#), *npj Clean Water*, **5**: 5 (2022).
- [31] Luo T., Wang M., Tian X., Nie Y., Yang C., Lin H.M., Luo W., Wang Y., [Safe and Efficient Degradation of Metronidazole Using Highly Dispersed B-FeOOH on Palygorskite Ashheterogeneous Fenton-Like Activator of Hydrogen Peroxide](#), *Chemosphere*, **236**: 124367 (2019).
- [32] Xu L., Wang J., [A Heterogeneous Fenton-Like System with Nanoparticulate Zero-Valent Iron for Removal of 4 Chloro-3-Methyl Phenol](#), *J. Hazard. Mater.*, **186**: 256-264 (2011).
- [33] Deng J., Dong H., Zhang C., Jiang Z., Cheng Y., Hou K., Zhang L., Fan C., [Nanoscale Zero-Valent Iron/Biochar Composite as An Activator for Fenton-Like Removal of Sulfamethazine](#), *Sep. Purif. Technol.*, **202**: 130-137 (2018).
- [34] Lin C.C., Hsu S.T., [Performance of nZVI/H<sub>2</sub>O<sub>2</sub> Process in Degrading Polyvinyl Alcohol in Aqueous Solutions](#), *Sep. Purif. Technol.*, **203**: 111-116 (2018).

- [35] Bae S., Kim D., Lee W., [Degradation of Diclofenac by Pyrite Catalyzed Fenton Oxidation](#), *Appl. Catal., B*, **134-135**: 93-102 (2013).
- [36] Wang L., Yang J., Li Y., Lv J., Zou J., [Removal of Chlorpheniramine in A Nanoscale Zero Valent-Iron Induced Heterogeneous Fenton System: Influencing Factors and Degradation Intermediates](#), *Chem. Eng. J.*, **284**: 1058-1067 (2016).
- [37] Yan X., Qinggang Z., Guang L., Xiaobo T., Yuanquan Z., Xiaohong H., [Biodegradability Enhancement of Real Antibiotic Metronidazole Wastewater by A Modified Electrochemical Fenton](#), *J. Taiwan Inst. Chem. Eng.*, **96**: 256-263 (2019).
- [38] Chen J., Qiu X., Fang Z., Yang M., Pokeung T., Gu F., Cheng W., Lan B., [Removal Mechanism of Antibiotic Metronidazole from Aquatic Solutions by Using Nanoscale Zero-Valent Iron](#), *Chem. Eng. J.*, **181-182**: 113-119 (2012).

UCCF-Accepted Article